

The sub-damped Ly α system toward HE 0001–2340: galaxy formation at $z \approx 2$ ^{*}

P. Richter¹, C. Ledoux², P. Petitjean³, and J. Bergeron³

¹ Institut für Astrophysik und Extraterrestrische Forschung, Auf dem Hügel 71, 53121 Bonn, Germany
e-mail: prichter@astro.uni-bonn.de

² European Southern Observatory, Alonso de Córdova 3107, Casilla 19001, Vitacura, Santiago, Chile

³ Institut d’Astrophysique de Paris – CNRS, 98bis Boulevard Arago, 75014 Paris, France

Received 24 September 2004 / Accepted 11 May 2005

Abstract. We present a detailed analysis of chemical abundances in a sub-damped Ly α absorber (sub-DLA) at $z = 2.187$ towards the quasar HE 0001–2340 ($z_{\text{em}} = 2.28$). Our study is based on high-resolution ($R \approx 45\,000$) spectroscopic data from the UVES instrument installed on the ESO *Very Large Telescope* (VLT). This sub-DLA system consists of at least 25 individual subcomponents spanning a restframe velocity range of $\sim 400\text{ km s}^{-1}$. The total neutral hydrogen column density is $\log N(\text{HI}) \approx 19.7$. Detected species include C II, C IV, N I, N II, O I, Mg II, Al II, Al III, Si II, Si IV, P II, Fe II, and possibly D I. For the dominating neutral gas component at $v_{\text{rel}} = +13\text{ km s}^{-1}$ (relative to $z = 2.187$) we derive an oxygen abundance of $[\text{O}/\text{H}] = -1.81 \pm 0.07$ (1/65 solar). With its extremely low nitrogen content ($[\text{N}/\text{H}] \lesssim -3.3$ and $[\text{N}/\text{O}] \lesssim -1.5$) the absorber exhibits a classic massive star abundance pattern. Our measurements place the $z = 2.187$ absorber towards HE 0001–2340 among the systems with the lowest ever measured $[\text{N}/\alpha]$ ratios. The low $[\text{N}/\text{O}]$ value is consistent with the idea that primary nitrogen production by the very first stars have enriched the intergalactic gas to a level of $[\text{N}/\text{O}] \approx -1.5$. Peculiar abundances are found in the outermost blue components near -350 km s^{-1} (in the $z = 2.187$ restframe) where we observe significant overabundances of phosphorus ($[\text{P}/\text{C}] \approx +1.5$), silicon ($[\text{Si}/\text{C}] \approx +0.6$), and aluminum ($[\text{Al}/\text{C}] \approx +0.5$) after correcting for the effects of ionization. Our study suggests that the line of sight passes through the gaseous environment of one or more stellar clusters that locally enriched their interstellar neighbourhood by supernova ejecta generating the observed abundance anomalies. The large velocity spread of the entire absorption system points to a merger that triggers the formation of these clusters. We thus may be observing a young galaxy at $z \approx 2$ that is forming out of a merger event.

Key words. cosmology: observations – Galaxy: abundances – Galaxy: evolution – quasars: absorption lines

1. Introduction

Absorption line systems at high redshift provide a wealth of information about the chemical evolution of the early Universe. Next to the Ly α forest and the Lyman limit systems that trace the low-density IGM or the intergalactic environment of galaxies at neutral hydrogen column densities of $N(\text{HI}) < 10^{19}\text{ cm}^{-2}$, the physical and chemical properties of absorbers with $N(\text{HI}) \geq 10^{19}\text{ cm}^{-2}$ are particularly interesting. These systems contain most of the neutral gas mass in the Universe at $z > 1$ (Lanzetta et al. 1995; Wolfe et al. 1995) and consist of heavy elements in an abundance pattern that suggests the chemical enrichment by the first generations of stars (e.g., Lu et al. 1996; Prochaska & Wolfe 1999). Such absorbers therefore may represent progenitors of present-day galaxies.

Most of the information about abundances of metals, dust and molecules in these systems has been obtained from the

damped Ly α systems (DLAs), which have HI column densities $> 2 \times 10^{20}\text{ cm}^{-2}$ (e.g., Ledoux et al. 2003). Absorption systems with somewhat lower column densities ($10^{19}\text{ cm}^{-2} \leq N(\text{HI}) \leq 2 \times 10^{20}\text{ cm}^{-2}$) are the so-called sub-damped Ly α systems (sub-DLAs; e.g., Dessauges-Zavadsky et al. 2003; Péroux et al. 2003). While there is no compelling evidence that DLAs and sub-DLAs trace different classes of protogalactic objects, abundance measurements in sub-DLAs are of particular interest because of their absorption characteristics. For total HI column densities $\leq 2 \times 10^{20}\text{ cm}^{-2}$ and metallicities less than ~ 0.1 solar, the absorption lines from neutral oxygen and neutral nitrogen (two important elements for disentangling the complex chemical enrichment history of high- z absorbers) are relatively weak. This enables us to derive accurate abundances for these two important elements in sub-DLAs without facing the problem of heavy line saturation in the oxygen lines.

In this paper we present the detailed analysis of a sub-damped Ly α system at $z = 2.187$ in the direction of the quasar HE 0001–2340. This paper represents the first in a series of two papers dealing with the chemical and physical properties

^{*} Based on observations carried out at the European Southern Observatory (ESO), La Silla, under prog. ID No. 166.A-0106 with the UVES spectrograph at the ESO Very Large Telescope, Paranal, Chile.

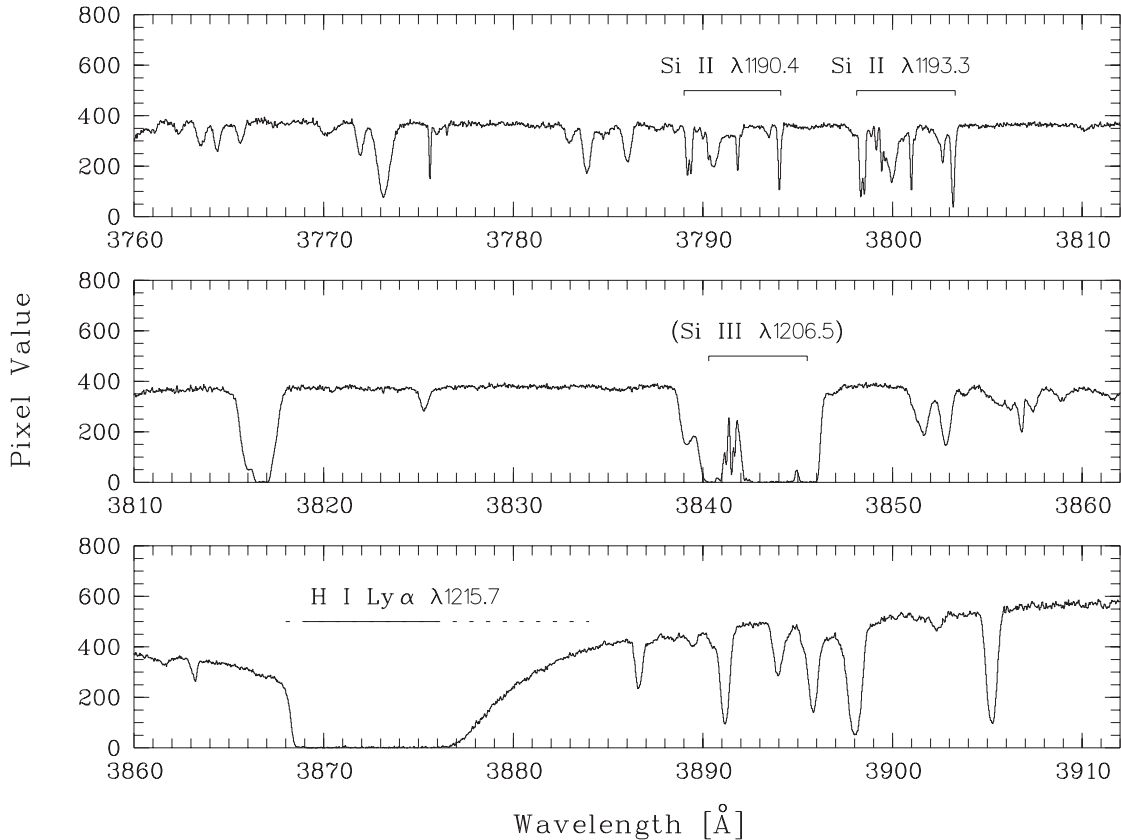


Fig. 1. Portion of the UVES spectrum of HE 0001–2340 in the wavelength range between 3760 and 3912 Å. Absorption by Si II $\lambda\lambda 1190.4, 1193.3$, Si III $\lambda 1206.5$ (blended by intervening H I) and H I Ly $\alpha \lambda 1215.7$ from the $z = 2.187$ sub-DLA is shown in the upper, middle and lower panel, respectively.

of particularly interesting sub-DLA systems in the data set of the ESO-VLT Large Programme “The Cosmic Evolution of the IGM”. This paper is organized as follows: in Sect. 2 we present the observations, the data reduction and the data analysis method. Absorption by neutral and weakly ionized species is presented in Sect. 3. Section 4 deals with the properties of the highly ionized gas. We discuss the results in Sect. 5 and summarize our study in Sect. 6.

2. Observations, data handling and analysis method

The quasar HE 0001–2340 ($V = 16.7$, $z_{\text{em}} = 2.28$) was observed with the UVES instrument installed on the VLT as part of the ESO-VLT Large Programme “The Cosmic Evolution of the IGM”, which aims at providing a homogeneous data set of high-resolution ($R \sim 45\,000$), high signal-to-noise ($S/N > 30$) spectral data for QSO absorption line spectroscopy of the IGM in the redshift range between $z = 2.2$ – 4.5 .

HE 0001–2340 was observed through a $1''$ slit (with a seeing typically $\leq 0.8''$) with two setups using dichroic beams splitters for the blue and the red arm (Dic 1, B346 nm+R580 nm, and Dic 2, B437 nm+860 nm, respectively). This setup provides a wavelength coverage from ~ 3050 to $10\,400$ Å, with small gaps near 5750 and 8550 Å. The total integration time (Dic 1 + Dic 2) for HE 0001–2340 was 12 h. The raw data were reduced using the UVES pipeline

implemented in the ESO-MIDAS software package. The pipeline reduction includes flat-fielding, bias- and sky-subtraction and a relative wavelength calibration. The individual spectra then have been coadded and corrected to vacuum wavelengths. The S/N in the spectrum generally is very high and attains a maximum of ~ 150 per resolution element for $\lambda > 4000$ Å. In Fig. 1, a representative portion of the UVES spectrum of HE 0001–2340 in the wavelength range between 3760 and 3912 Å is displayed, showing selected absorption lines of the sub-DLA system at $z = 2.187$.

For the spectral analysis of the data we made use of the FITLYMAN package in MIDAS (Fontana & Ballester 1995). This routine uses a χ^2 minimization algorithm to derive column densities, N , and Doppler-parameters, b , via Voigt-profile fitting, taking into account the spectral resolution of the instrument (see above). First, we have disentangled the component structure in the $z = 2.187$ absorber for a) neutral and weakly ionized species (singly ionized species plus Al III), and b) highly ionized species (C IV and Si IV), as explained in detail in Sects. 3 and 4. Using a number of high S/N absorption profiles from various species we then obtained Doppler parameters for each component by Voigt profile fitting. We use a single b value per absorption component to fit all neutral and weakly ionized species except hydrogen and deuterium. Figure 2, lower panel, shows an example for a Voigt profile fit to the Al II $\lambda 1670.8$ line. The spectral data are plotted with black points, the corresponding fit is shown as solid

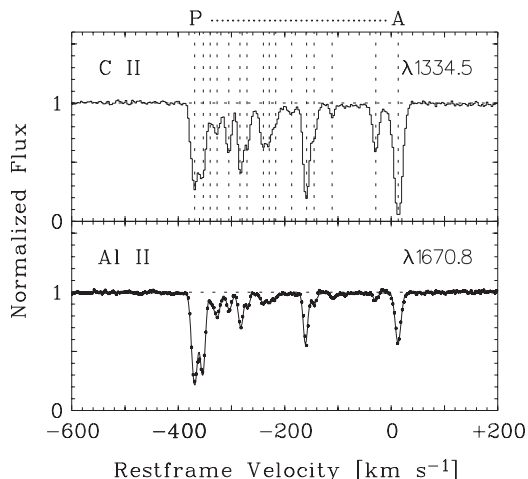


Fig. 2. Absorption profiles of C II and Al II from the $z = 2.187$ sub-DLA are displayed (velocities refer to the $z = 2.187$ restframe). The C II $\lambda 1334.5$ absorption (upper panel) demonstrates the complex velocity structure of this absorber. 16 individual components are identified, given by the letters A to P. These components are indicated by the vertical dashed lines. The lower panel shows an example for a multi-component Voigt profile fit from the FITLYMAN routine. Absorption by Al II $\lambda 1670.8$ (dots) is overlaid with the corresponding optimum fit (solid line).

line. Throughout this paper we use wavelengths and oscillator strengths from the atomic line list of Morton (2003).

3. Neutral and weakly ionized species

3.1. Velocity structure and b values

Figure 2 (upper panel) shows the C II $\lambda 1334.5$ line plotted on the $z = 2.187$ restframe velocity scale, demonstrating the complex component structure of this absorption system. The C II line, among others, is sufficiently strong to show also weak velocity components and lies in a region that is not affected by line blending. Moreover, this line has a high S/N , so that the various subcomponents can be reliably identified. To derive a unique model for the velocity component structure we have fitted Voigt profiles to a number of high S/N lines of C II, Mg II, and Si II. We identify 16 velocity subcomponents, in Fig. 2 shown with vertical dashed lines. In the $z = 2.187$ restframe these absorption components have relative velocities of +13, -29, -111, -145, -159, -187, -217, -229, -240, -271, -284, -305, -327, -340, -353, and -369 km s^{-1} . This velocity model then has been used to derive b values and column densities for each component via Voigt-profile fitting. The resulting values for b and $\log N$ and their 1σ errors are listed in Table 1. Throughout the following, we label the individual velocity components with the letters A to P in alphabetical order (i.e., component A is the one at +13 km s^{-1}). The strongest absorption in C II and other neutral and weakly ionized species is seen in component A, thus at the outermost red wing of the overall absorption structure.

3.2. Metals

A number of neutral and weakly ionized species are detected in the various velocity components, including C II, N I, N II, O I, Mg II, Al II, Al III, Si II, P II, and Fe II. A selection of

velocity profiles of these species is shown in Fig. 3. Column densities for these ions as well as upper limits for undetected species (e.g., Zn II, S II and molecular hydrogen, H_2) are listed in Table 1. The strong lines of C II ($\lambda\lambda 1334.5, 1036.3$) and Mg II ($\lambda\lambda 2803.5, 2796.4$) are saturated in the dominating neutral components A, E, K, O and P. As there are no weaker transitions available for these species, the column densities derived for C II and Mg II in these components are relatively uncertain (see Table 1). For O I, N I, Al II, Al III, Si II and Fe II unsaturated lines are available that allow us to derive accurate column densities from profile fitting. N I absorption is detected solely in component A. The measured equivalent width of the N I feature in the $\lambda 1199.6$ line (see Fig. 3, third panel in the left row) is only 1.8 mÅ, corresponding to a 3.0σ significance at the measured local S/N of ~ 130 per resolution element. The detection of P II in the outermost blue components O and P, as shown in Fig. 4, is remarkable. This is surprising, since P II has a relatively low cosmic abundance ($\log (P/H)_\odot = -6.44$) and is not observed in the strongest neutral component A.

3.3. Neutral hydrogen absorption

Neutral hydrogen absorption in the $z = 2.187$ sub-DLA is seen in Ly α , Ly β and Ly γ , as shown in Fig. 5. The other lines from the H I Lyman series either have very low S/N or are located bluewards of the available UVES wavelength range. As clearly visible in Figs. 1 and 5, the Ly α absorption is very asymmetric due to the large number of neutral gas components at the blue side that contribute to the overall H I absorption. The red part of the Ly α absorption shows a well-defined damping wing caused by the strongest neutral gas component at +13 km s^{-1} (component A). Due to the asymmetry, a free single-component fit of the Ly α , Ly β , and Ly γ absorption cannot even roughly reproduce the observed shape of the absorption. Therefore, the complex velocity structure of the $z = 2.187$ absorber has to be taken into account for the profile fit of the H I Lyman series absorption. Fixing the centroid of the fit at +13 km s^{-1} and only fitting the damping wing on the red side of the Ly α , Ly β and Ly γ absorption simultaneously results in an H I column density of $\log N(\text{H I})_A = 19.60 \pm 0.4$ for component A. Similarly, we can constrain the total H I column density in the two bluest velocity components O and P to $\log N(\text{H I})_{OP} \leq 18$ by fixing the velocity centroid at -361 km s^{-1} and fitting the blue wing of the Ly β and Ly γ absorption. Note that the additional absorption occurring in the blue wing of the Ly α , Ly β , and Ly γ absorption is possibly due to deuterium (D I) in components O and P in combination with an additional weak H I component near -440 km s^{-1} . This will be further discussed in the Appendix.

The entire H I absorption in the Ly α , Ly β and Ly γ profile can be modeled by taking into account the absorption from the intermediate velocity components. For our model, we consider absorption from the strongest neutral gas components A, B, E, K, L, O, and P, for which we have fixed the velocity-component structure as seen in the metal-line absorption. The presence of a residual flux spike in the Ly β profile near -300 km s^{-1} is characteristic and needs to be reproduced by our model. A similar spike is not seen in the Ly γ absorption profile, but it is likely

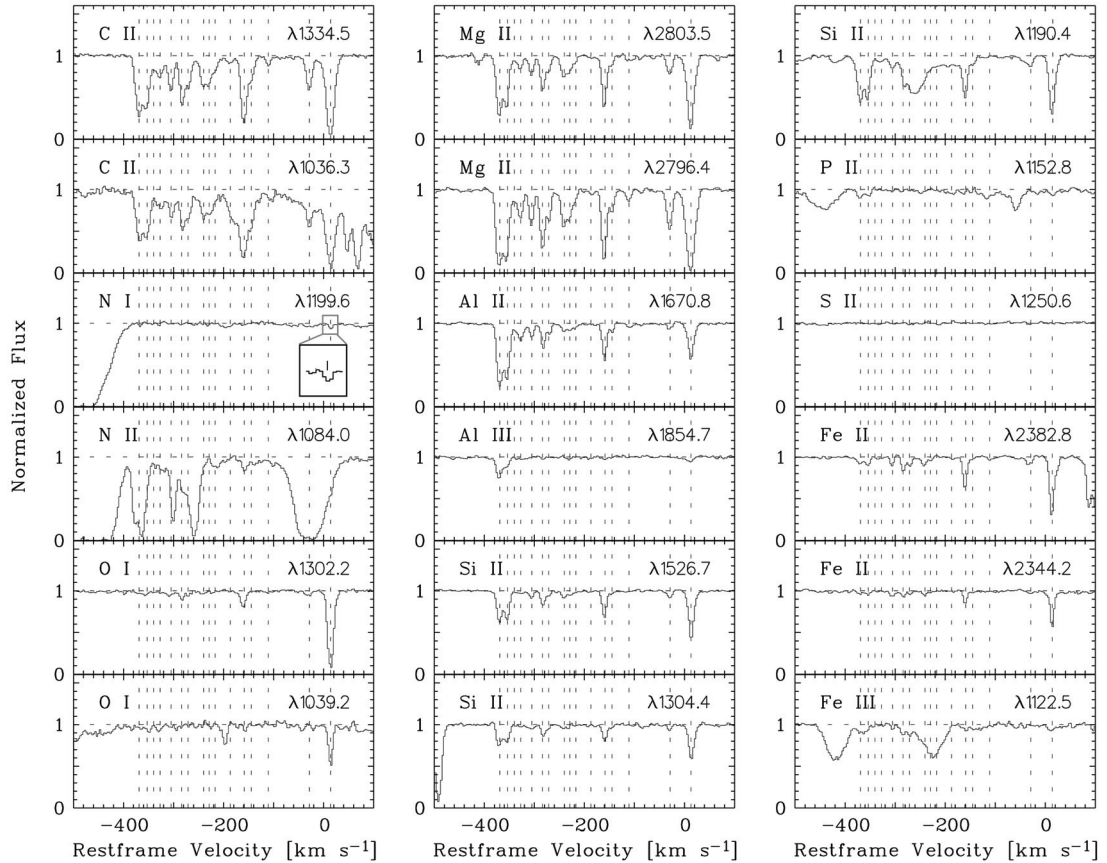


Fig. 3. Absorption profiles of C II, N I, N II, O I, Mg II, Al II, Al III, Si II, P II, S II, Fe II and Fe III for the $z = 2.187$ sub-DLA are shown. The individual absorption components are indicated with the vertical dashed lines. The velocity scale refers to the $z = 2.187$ restframe.

that in this region the Ly γ line is blended with absorption from the Ly α forest. The best fitting model has logarithmic HI column densities of 19.60, 17.79, 18.25, 15.03, 17.71, 17.53 and 17.32 for the components A, B, E, K, L, O and P, respectively. This model is shown Fig. 5 with a thick solid line; the expected flux spike near -300 km s^{-1} in the Ly γ absorption is indicated with a thick dashed line. Note that this fit for the intermediate velocity components is not unique, as other combinations of HI column densities also can reproduce the shape of the observed HI absorption. An important outcome of this model is, however, that the absorption of the intermediate components does not significantly influence the shape of the HI absorption in the blue and red wing of the Lyman lines. Therefore, the values of $\log N(\text{HI})_A = 19.60 \pm 0.4$ and $\log N(\text{HI})_{OP} \leq 18$ derived above represent reliable estimates for the HI column densities in components A and O+P.

3.4. Abundances and abundance ratios

3.4.1. Component A

First, we concentrate on the dominating neutral component (component A) in our discussion of abundances and abundance ratios in the $z = 2.187$ absorber. The best element to derive the overall abundance in the gas is oxygen, since neutral oxygen and neutral hydrogen have similar ionization potentials and both elements are coupled by a strong charge-exchange

reaction. Moreover, oxygen does not deplete significantly into dust grains. Our analysis yields $[\text{O}/\text{H}] = -1.81 \pm 0.07^1$, which corresponds to an abundance of $\sim 1/65$ solar. In striking contrast, the nitrogen abundance is significantly lower, $[\text{N}/\text{H}] = -3.50 \pm 0.05$ or $\sim 1/3200$ solar, as derived from N I. The resulting nitrogen-to-oxygen ratio $[\text{N}/\text{O}] = -1.69$, if accurate, would be one of the lowest ever measured in DLAs so far. However, the interpretation of N I/H I is not as straightforward as for O I/H I. Although the ionization potential of N I is only slightly higher than that of hydrogen (14.53 versus 13.60 eV), ionization effects can significantly affect the determination of $[\text{N}/\text{H}]$ from N I and H I in absorbers with overall column densities $\leq 10^{20} \text{ cm}^{-2}$. The reason for this is that charge exchange reactions are less efficient between N I and H I (in contrast to O I and H I; see Butler & Dalgarno 1979) and N I has a relatively large photoionization cross section (Sofia & Jenkins 1998). Thus, a considerable fraction of the nitrogen in component A may reside in the N^+ phase, particularly if a substantial ionizing radiation field is present. While the uncertain column density constraint from the blended N II $\lambda 1084.0$ line ($\log N(\text{N II}) \leq 12.80$) does not provide a very stringent estimate of the abundance of singly ionized nitrogen, we can check possible ionization effects in component A using other weakly ionized species. The ratio of $(\text{Al III}/\text{Al II}) \approx 0.3$ suggests that ionization could be important. This ratio, however, is difficult

¹ $[\text{X}/\text{H}] = \log(\text{X}/\text{H}) - \log(\text{X}/\text{H})_\odot$.

Table 1. Logarithmic ion column densities and b values for the $z = 2.187$ absorber towards HE 0001-2340.

Comp.	v_{rel} [km s ⁻¹]	z_{abs}	Ion	$\log N^a$	b^a [km s ⁻¹]	Comp.	v_{rel} [km s ⁻¹]	z_{abs}	Ion	$\log N^a$	b^a [km s ⁻¹]								
A	+13	2.18714	C II	14.36 ± 0.19	4.5 ± 0.8	I	-240	2.18445	C II	13.03 ± 0.05	4.8 ± 1.3								
			N I	12.05 ± 0.03					Mg II	12.23 ± 0.05									
			N II	≤12.80					Al II	11.23 ± 0.04									
			O I	14.48 ± 0.05					Si II	12.31 ± 0.04									
			Mg II	13.13 ± 0.10					Fe II	11.80 ± 0.05									
			Al II	11.98 ± 0.04															
			Al III	11.45 ± 0.04					J	-271		2.18412	C II	13.11 ± 0.05	5.8 ± 1.1				
			Si II	13.35 ± 0.04									Mg II	12.07 ± 0.05					
			P II	≤12.02									Al II	11.28 ± 0.05					
			S II	≤13.12									Si II	12.11 ± 0.05					
			Fe II	12.98 ± 0.03									Fe II	11.76 ± 0.05					
			B	-29					2.18669	C II		13.20 ± 0.04	6.0 ± 1.0	K	-284	2.18398	C II	13.40 ± 0.03	4.5 ± 1.0
										O I		12.67 ± 0.05					O I	12.85 ± 0.05	
Mg II	12.07 ± 0.04	Mg II			12.46 ± 0.04														
Al II	11.06 ± 0.05	Al II			11.71 ± 0.04														
Si II	12.32 ± 0.03	Al III			11.05 ± 0.03														
Fe II	11.80 ± 0.05	Si II			12.56 ± 0.05														
		Fe II			11.99 ± 0.04														
C	-111	2.18582	C II	12.43 ± 0.03	3.0 ± 0.8	L	-305	2.18376	C II	13.17 ± 0.05	4.9 ± 0.7								
			Mg II	11.83 ± 0.03					O I	12.58 ± 0.06									
			Al II	10.89 ± 0.04					Mg II	12.17 ± 0.03									
			Si II	11.31 ± 0.04					Al II	11.41 ± 0.03									
D	-145	2.18546	C II	12.96 ± 0.06	5.0 ± 1.1	M	-327	2.18352	C II	12.63 ± 0.06	5.0 ± 1.7								
			Mg II	11.88 ± 0.06					Mg II	11.93 ± 0.05									
			Al II	11.28 ± 0.03					Al II	11.49 ± 0.05									
			Si II	12.16 ± 0.04					Si II	11.76 ± 0.05									
E	-159	2.18531	C II	13.94 ± 0.10	3.1 ± 0.9	N	-340	2.18339	C II	12.59 ± 0.09	6.4 ± 2.5								
			N II	≤12.82					Mg II	11.63 ± 0.07									
			O I	13.13 ± 0.04					Al II	11.26 ± 0.06									
			Mg II	12.81 ± 0.06					Si II	11.73 ± 0.05									
			Al II	11.93 ± 0.03															
			Al III	11.09 ± 0.04					O	-353		2.18325	C II	13.56 ± 0.09	4.3 ± 1.3				
			Si II	12.88 ± 0.03									O I	12.41 ± 0.05					
			Fe II	12.35 ± 0.03									Mg II	12.76 ± 0.05					
Fe III	≤12.75	Al II	12.30 ± 0.05																
F	-187	2.18501	C II	13.02 ± 0.05	5.9 ± 1.4				Al III	11.83 ± 0.05									
			Mg II	11.46 ± 0.05		Si II	13.00 ± 0.04												
G	-217	2.18469	C II	12.75 ± 0.06	6.6 ± 2.3	P	-369	2.18308	C II	13.59 ± 0.07	5.1 ± 1.4								
			Mg II	11.79 ± 0.05					O I	≤12.34									
			Al II	10.99 ± 0.06					Mg II	12.87 ± 0.04									
			Si II	11.68 ± 0.07					Al II	12.44 ± 0.04									
H	-229	2.18457	C II	12.94 ± 0.10	3.5 ± 1.3				Al III	12.15 ± 0.04									
			Mg II	12.01 ± 0.07		Si II	13.08 ± 0.04												
			Al II	11.00 ± 0.05		P II	12.22 ± 0.04												
			Si II	11.95 ± 0.05		Fe II	≤11.82												
			Fe II	11.53 ± 0.04		Fe III	≤12.81												

^a 1 σ errors and 3 σ upper limits are given.

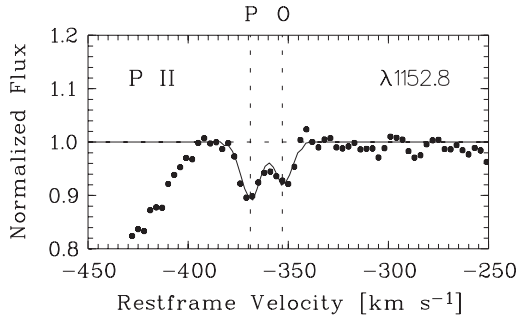


Fig. 4. Zoomed-in version of P II $\lambda 1152.8$ absorption in the $z = 2.187$ absorber in the range between -450 and -250 km s $^{-1}$. P II absorption in components O and P (indicated by the dashed lines) is clearly detected. The solid line shows the optimum two-component Voigt-profile fit.

to interpret due to the uncertain recombination rate of Al $^{+}$ (see Vladilo et al. 2001; Nussbaumer & Storey 1986) and the observed discrepancies between (Al III/A II) and other ionic ratios in high- z photoionization models (e.g., D’Odorico & Petitjean 2001). An important element to investigate ionization conditions in interstellar and intergalactic gas is the α element sulfur (Richter et al. 2001). S II has an ionization potential of 23.23 eV and depletes only very little into dust, so that we expect most S to be in the form of S II. Since the ionization potential of S II is significantly higher than that of O I and H I (~ 13.6 eV for both), S II exists in gas where part of the hydrogen is ionized. From the observed S II/O I ratio we thus can learn about the hydrogen ionization fraction (see Richter et al. 2001 for details). Although S II is not detected in our sub-DLA, the 3σ upper limit for the S II column density in component A ($\log N(\text{S II}) \leq 13.12$) yields $[\text{S}/\text{H}] \leq -1.68$ and $[\text{S II}/\text{O I}] \leq +0.13$. If one assumes a solar sulfur-to-oxygen ratio, the possible small excess of S II compared to O I implies that the degree of ionization in component A is low (<30 percent)². We conclude that N II/N I most likely is small, so that we can give a conservative limit for the nitrogen abundance in component A of $[\text{N}/\text{H}] \lesssim -3.3$ and $[\text{N}/\text{O}] \lesssim -1.5$.

The apparently low degree of ionization in combination with the equal abundances of Si and O speaks against any significant dust depletion of silicon in component A. The situation is somewhat less clear for the elements Mg, Al and Fe, which are all underabundant compared to oxygen ($[\text{Mg}/\text{O}] = -0.24$, $[\text{Al}/\text{O}] = -0.30$ and $[\text{Fe}/\text{O}] = -0.31$). These elements could be depleted into dust grains. In fact, with $[\text{Fe}/\text{O}] = -0.31$ and $[\text{Si}/\text{O}] = 0.00$ the absorber follows the trend for dust depletion patterns found in damped Ly α systems and in the Galactic halo (see Petitjean et al. 2002, their Fig. 7). However, next to dust depletion, nucleosynthesis effects certainly have to be considered for these elements given the low overall abundance and the very low nitrogen content. In this context, the observed abundances of iron and aluminum could also be explained by a slightly enhanced $[\alpha/\text{Fe}]$ element ratio and a mild

² Note that if the intrinsic S/O ratio in this system is significantly lower than solar, the ionization fraction would be underestimated by this method. Some DLAs indeed show sub-solar S/O ratios (e.g., Prochaska et al. 2003).

odd-even effect for Al. In contrast to Fe and Al, the column density of magnesium unfortunately is too uncertain (due to saturation of the two available Mg II lines) to draw meaningful conclusions about the apparent Mg underabundance. The absence of molecular hydrogen absorption in component A represents yet another piece of information on the dust abundance in the gas. From the H $_2$ column density limit (see Table 1) we obtain an upper limit for the molecular hydrogen fraction of $f = [2N(\text{H}_2)/(N(\text{H I}) + 2N(\text{H}_2))] \approx 5 \times 10^{-7}$. As H $_2$ preferentially forms on the surfaces of dust grains, the lack of H $_2$ further supports the above conclusion that the dust abundance in component A must be small (see also Ledoux et al. 2003). Little can be said about the carbon abundance in component A, as the value of $[\text{C}/\text{H}] = -1.76 \pm 0.21$ – although similar to that of oxygen – is very uncertain due to saturation of the two C II lines. If the b value would be only slightly higher than the assumed 4.5 km s $^{-1}$, the C II column density (and thus the derived carbon abundance) would drop substantially.

All measured abundances in component A are summarized in Table 2.

3.4.2. Components O and P

We now turn to components O and P, which show a very distinct abundance pattern. As discussed in Sect. 3.3, the Ly α Voigt profile fit yields $\log N(\text{H I}) \leq 18$ for components O and P together. The combined O I column density for O and P is $\log N \approx 12.7$ (see Table 1), from which we infer an oxygen abundance of $[\text{O}/\text{H}]_{\text{OP}} \geq -2.0$. This is consistent with the oxygen abundance derived for component A. The large value for $\log (\text{C II}/\text{O I}) = +1.15$ in component O implies that the degree of ionization must be large. Note that the C II absorption in components O and P is not saturated (unlike in component A), so that the derived C II column densities are accurate (see Table 1). From C II, Mg II, Si II, Al II and P II we obtain $(\text{Mg II}/\text{C II})_{\text{OP}} = -0.76$, $(\text{Si II}/\text{C II})_{\text{OP}} = -0.54$, $(\text{Al II}/\text{C II})_{\text{OP}} = -1.21$ and $(\text{P II}/\text{C II})_{\text{OP}} = -1.45$. From Fe II and Fe III we derive $(\text{Fe II}+\text{Fe III})/\text{C II})_{\text{OP}} = -0.74$. These ratios suggest significant overabundances of silicon, aluminum and phosphorus in components O and P. However, a confirmation of this statement and a more quantitative estimate of the apparent overabundances has to await a detailed photoionization modeling for these species. This will be presented in Sect. 4.2.

4. Highly-ionized species

4.1. Component structure and column densities

Absorption by highly ionized gas in the $z = 2.187$ absorber is seen in C IV $\lambda\lambda 1550.8, 1548.2$ and Si IV $\lambda\lambda 1402.8, 1393.3$. O VI and N V are not detected, but blending problems hamper a reliable detection of these ions. The component structure seen in C IV and Si IV (Fig. 6) is even more complex than that of the neutral and weakly ionized gas. All in all, we identify 25 absorption components including the 16 components detected in neutral and weakly ionized species. All C IV and Si IV measurements are summarized in Table 3.

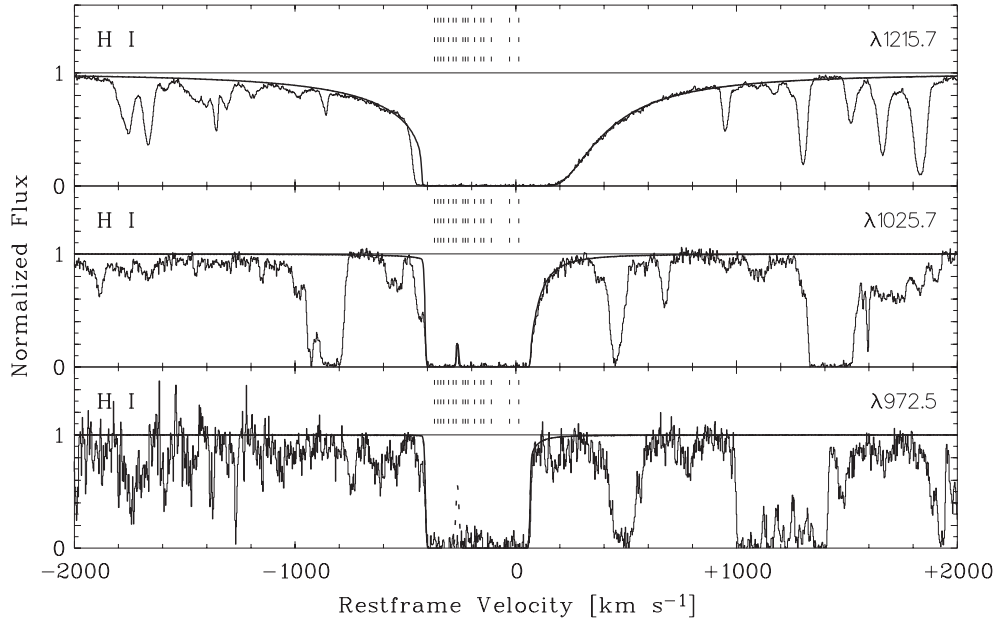


Fig. 5. H I Ly α , Ly β , and Ly γ absorption in the $z = 2.187$ absorber. The thick solid line represents the best-fitting H I model, as described in Sect. 3.3.

Table 2. Summary of logarithmic metal abundances in component A.

Species	I.P. [eV]	$\log (X/H)_{\odot}^a$ (+12)	$[X/H]^b$
C II	24.38	8.52	-1.76 ± 0.21
N I	14.53	7.95	-3.50 ± 0.05
N II	29.60	7.95	≤ -2.75
O I	13.62	8.69	-1.81 ± 0.07
Mg II	15.04	7.58	-2.05 ± 0.11
Al II	18.83	6.49	-2.11 ± 0.06
Al III	28.45	6.49	-2.64 ± 0.06
Si II	16.35	7.56	-1.81 ± 0.07
P II	19.77	5.56	≤ -1.18
S II	23.34	7.20	≤ -1.68
Fe II	16.19	7.50	-2.12 ± 0.05
Fe III	30.65	7.50	≤ -2.23
Zn II	17.96	4.67	≤ -1.23

^a Reference abundances are taken from Allende Prieto et al. (2001) for oxygen and from the compilation of Morton (2003) and references therein.

^b $[X/H] = \log (X/H) - \log (X/H)_{\odot}$.

4.2. Photoionization modeling for comp. O and P

Our measurements of C II, C IV, Si II and Si IV allow us to model the photoionization in components O and P and to constrain the ionization parameter $U = n_{\gamma}/n_{\text{H}}$, the ratio of ionizing photon density to gas density. We have used the photoionization code CLOUDY v94.00 (Ferland 1996) and have modeled a plane-parallel slab of gas with a metallicity of 0.01 solar and solar relative chemical abundances (Fig. 7). The calculations were done using a constant density and were stopped whenever the neutral hydrogen column density reached 10^{18} cm^{-2} . The total hydrogen column density in the model, $N(\text{H I} + \text{H II})$,

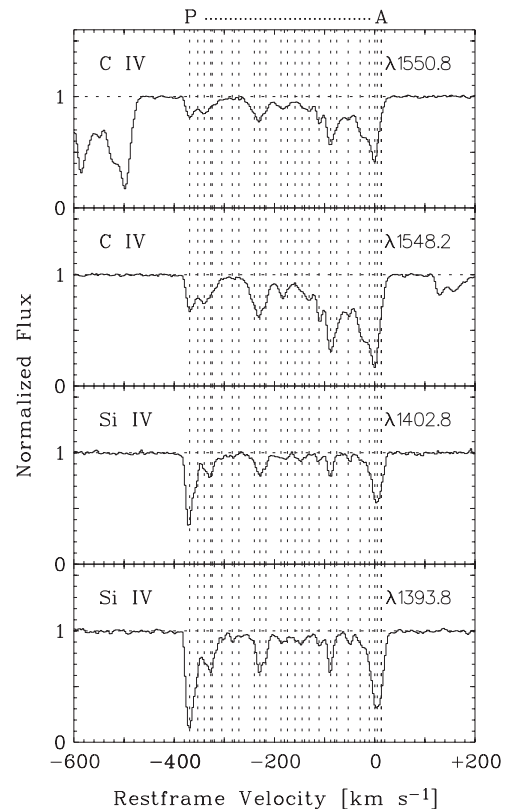
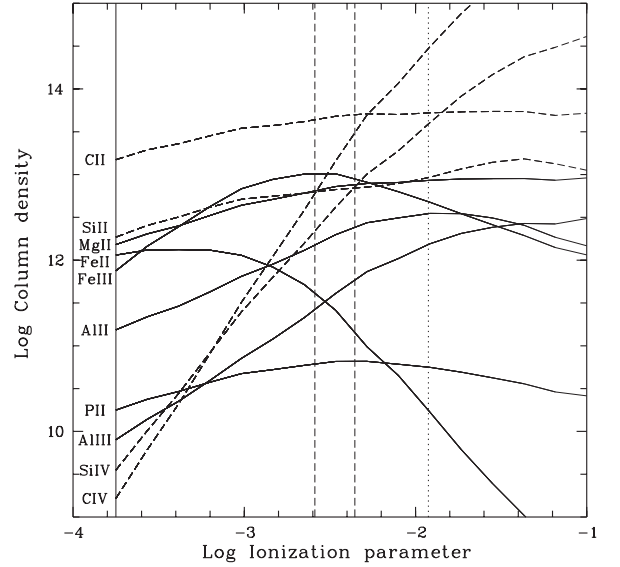


Fig. 6. Absorption by C IV ($\lambda\lambda 1550.8, 1548.2$) and Si IV ($\lambda\lambda 1402.8, 1393.8$) in the $z = 2.187$ absorber is shown. The absorption pattern of these high ions is even more complex than for the neutral and weakly ionized species. We identify 25 components that partly correspond to the absorption components seen in C II (see also Table 3, for details).

comes out to $1.0 \times 10^{20} \text{ cm}^{-2}$. For the ionizing radiation, we used the Madau et al. (1999) metagalactic spectrum at

Table 3. Logarithmic column densities for C IV and Si IV.

Comp.	v_{rel} [km s ⁻¹]	z_{abs}	Ion	$\log N^a$	b^a [km s ⁻¹]
A	+13	2.18714	C IV	12.01 ± 0.05	4.5 ± 0.7
			Si IV	12.28 ± 0.04	5.6 ± 0.4
A1	+5	2.18705	Si IV	13.01 ± 0.03	9.4 ± 1.1
A2	0	2.18700	C IV	13.58 ± 0.04	9.7 ± 1.4
A3	-11	2.18688	Si IV	12.52 ± 0.08	18.5 ± 3.6
B	-29	2.19669	C IV	13.48 ± 0.06	14.6 ± 2.7
B1	-53	2.18644	C IV	12.84 ± 0.11	11.6 ± 4.4
			Si IV	12.11 ± 0.14	3.5 ± 1.8
B2	-76	2.18619	C IV	13.02 ± 0.12	8.8 ± 4.9
B3	-88	2.18606	C IV	13.22 ± 0.07	6.8 ± 0.9
			Si IV	12.45 ± 0.04	4.7 ± 0.3
C	-111	2.18582	C IV	12.93 ± 0.06	6.5 ± 0.8
			Si IV	11.85 ± 0.05	4.9 ± 1.3
C1	-131	2.18561	C IV	12.63 ± 0.06	7.6 ± 1.1
D	-145	2.18546	C IV	12.40 ± 0.11	6.5 ± 2.4
			Si IV	11.74 ± 0.06	6.4 ± 1.8
E	-159	2.18531	Si IV	11.86 ± 0.23	15.4 ± 4.4
E1	-174	2.18515	C IV	11.65 ± 0.07	9.7 ± 2.0
F	-187	2.18501	C IV	12.72 ± 0.10	11.2 ± 2.1
			Si IV	11.90 ± 0.06	11.4 ± 1.7
G	-217	2.18469	C IV	12.75 ± 0.04	8.8 ± 1.8
			Si IV	12.06 ± 0.05	3.1 ± 1.1
H	-229	2.18457	C IV	12.90 ± 0.04	9.0 ± 1.3
			Si IV	12.49 ± 0.03	6.6 ± 0.5
I	-240	2.18445	C IV	12.58 ± 0.08	9.4 ± 2.2
			Si IV	11.80 ± 0.09	9.3 ± 1.5
J	-271	2.18412	Si IV	11.68 ± 0.13	9.8 ± 3.4
K	-284	2.18398	Si IV	11.55 ± 0.17	2.2 ± 1.6
L	-305	2.18376	Si IV	11.80 ± 0.10	5.0 ± 2.8
L1	-324	2.18356	Si IV	12.11 ± 0.08	4.1 ± 1.7
M	-327	2.18352	C IV	12.63 ± 0.05	14.2 ± 3.0
			Si IV	12.40 ± 0.07	9.0 ± 1.3
N	-340	2.18339	C IV	12.74 ± 0.05	9.5 ± 2.3
			Si IV	12.09 ± 0.04	2.0 ± 0.3
O	-353	2.18325	C IV	12.41 ± 0.07	8.9 ± 2.4
			Si IV	12.69 ± 0.05	7.2 ± 2.2
P	-369	2.18308	C IV	12.88 ± 0.06	8.5 ± 1.6
			Si IV	13.20 ± 0.04	5.5 ± 1.0

^a 1 σ errors and 3 σ upper limits are given.**Fig. 7.** CLOUDY photoionization model for several ions detected in components O and P. The model assumes an overall abundance of 0.01 solar together with a Madau et al. (1999) metagalactic ionizing spectrum for $z = 2.2$. The dashed vertical lines indicate the fits for the C IV/C II (left) and Si IV/Si II (right) column density ratios, the dotted vertical line indicates the fit for Al III/Al II (see Sect. 4.2 for details).

$z = 2.2$. Our CLOUDY modeling for the column density ratios of C IV/C II and Si IV/Si II implies ionization parameters of $\log U = -2.59$ and -2.35 , respectively, thus in good agreement with each other (see Fig. 7, vertical dashed lines). A value of $\log U \approx -2.5$ further is consistent with the observed column densities/column density limits for Fe II and Fe III. From the Al III/Al II ratio we obtain a significantly higher value of $\log U = -1.92$ (Fig. 7, vertical dotted line). This high value most likely is a result of the poorly known dielectric recombination rate of Al⁺ at high temperatures (Petitjean et al. 1994; Nussbaumer & Storey 1986) and therefore will not be considered any further here. Comparing the column densities predicted by the CLOUDY model with those measured allows us to constrain the metal abundances in components O and P. The results are summarized in Table 4. For oxygen, carbon, magnesium and iron we obtain abundances that are consistent with those measured in component A. For aluminum, silicon, and in particular for phosphorus, the CLOUDY model results in relative abundances that are significantly enhanced compared to solar. The overabundances relative to carbon amount to 0.5 ± 0.1 dex for aluminum, 0.6 ± 0.1 dex for silicon and 1.5 ± 0.1 dex for phosphorus (see Table 4).

5. Discussion

Our measurements of the sub-DLA at $z \approx 2.2$ towards HE 0001–2340 reveal a number of interesting abundance properties in this absorption system. With $[\text{O}/\text{H}] = -1.81 \pm 0.07$, $[\text{N}/\text{H}] \lesssim -3.3$ and $[\text{N}/\text{O}] \lesssim -1.5$ the sub-DLA towards HE 0001–2340 exhibits a classic massive star abundance pattern with little sign of primary nitrogen (e.g., Umeda & Nomoto 2004). While the alpha-element abundances $[\text{O}/\text{H}]$ and $[\text{Si}/\text{H}]$ are comparable to those measured for other sub-DLAs and

Table 4. Summary of logarithmic metal abundances in components O and P.

Species	$\log (X/H)_{\odot}^a$ (+12)	$[X/H]^b$	$[X/C]^b$
C	8.52	-1.9 ± 0.1	...
O	8.69	-2.0 ± 0.1	-0.1 ± 0.1
Mg	7.58	-1.7 ± 0.1	$+0.2 \pm 0.1$
Al	6.49	-1.4 ± 0.1	$+0.5 \pm 0.2$
Si	7.56	-1.3 ± 0.1	$+0.6 \pm 0.2$
P	5.56	-0.4 ± 0.1	$+1.5 \pm 0.1$
Fe	7.50	≤ -1.9	≤ 0.0

^a Reference abundances are taken from Allende Prieto et al. (2001) for oxygen and from the compilation of Morton (2003) and references therein.

^b Based on the CLOUDY photoionization model described in Sect. 4.2.

DLAs at similar redshifts (e.g., Dessauges-Zavadsky et al. 2002; Pettini et al. 2002), the $[N/\alpha]$ ($[N/O]$) ratio is among the lowest ever measured in DLAs and other astrophysical sites. $[N/\alpha]$ is a particularly important parameter to trace the chemical evolution in the early Universe. Nitrogen is believed to be produced mainly in intermediate-mass stars. The nitrogen deficiency observed in the intergalactic medium and in blue compact dwarf (BCD) galaxies (e.g., Prochaska et al. 2002; Izotov & Thuan 1999) probably is a result of the early chemical enrichment of type II supernovae from massive stars that produce only very little primary nitrogen. In low-metallicity environments with $[\alpha/H] \leq -1.5$, a first $[N/\alpha]$ plateau possibly is present near -1.5 dex, whereas for more metal-rich systems a second plateau occurs near -0.9 dex (Centurión et al. 2003). The region around $[N/\alpha] = -0.9$ is much more populated than the region near -1.5 dex, showing that most of observed environments must have experienced a second epoch of nitrogen and α -element enrichment after the initial enrichment to the $[N/\alpha] = -1.5$ level. In contrast to the -0.9 dex plateau, the one near -1.5 dex exhibits only small scatter (~ 0.05 dex) in (N/O) . To our knowledge, no systems with $[N/O]$ ratios ≤ -1.70 have been found so far. This may suggest that the value of $[N/O] \approx -1.5$ represents the lowest level for (N/O) in the Universe, set by the coeval injection of primary nitrogen and oxygen from the first generation of (massive) stars. The results presented here support this scenario. However, the number of systems with very low (N/O) values is still very limited and thus the existence of the -1.5 dex plateau still has to be confirmed by additional measurements (Centurión et al. 2003; Israelian et al. 2004).

Another interesting result of our study is the abnormal abundance pattern seen in components O and P. The ion column densities in these components derived in Sect. 3.4.2 and the CLOUDY model presented in Sect. 4.2 imply significant overabundances of aluminum (0.5 dex), silicon (0.6 dex) and phosphorus (1.5 dex) compared to carbon. Such an abundance pattern is highly unusual for DLAs. The findings may indicate that the line of sight towards HE 0001–2340 passes through a confined gaseous region in the DLA host that is locally polluted

with heavy elements by nearby supernova explosions. Since the ejecta of a single supernova do not contain enough material to significantly enhance the heavy metal abundance in larger volumes of interstellar gas, it seems plausible that the chemically enriched gas components O and P is related to massive (coeval) star-formation activity, such as in massive star clusters. Recent models for the so-called “hypernovae” (supernovae that have explosion energies $\geq 10^{52}$ erg) predict significantly enhanced $[Si/C]$ abundances in the supernova ejecta as a result of carbon and oxygen burning in low-density regions that lead to an enhanced freeze-out of α elements (e.g., Nakamura et al. 2001). Yet, these models cannot explain overabundances of phosphorus and aluminum and thus the exact explosion mechanism that may lead to the observed abundance pattern in components O and P remains unknown.

A striking feature of the $z = 2.187$ absorber towards HE 0001–2340 is the large number of individual velocity components that span a very large velocity range of almost ~ 400 km s⁻¹. This velocity span seems very large for a single (proto)galactic structure. One possible explanation for this is that the absorption pattern reflects a merger event of two galaxies or protogalactic structures. The individual velocity components that are quite narrow but that do not contain large columns of gas then may arise in tidal gaseous features produced by the merger event, spread out over a large spatial and radial-velocity range. An interesting aspect of a merger scenario lies in the idea that the merger actually *triggers* the formation of the stellar clusters (e.g., a nuclear cluster) that give rise to the abundance anomalies in components O and P. It is well known that merger/accretion events are of prime importance for starburst activity and the formation of massive stellar clusters in and around galaxies (e.g., Knierman et al. 2003; Schweizer & Seitzer 1998). If the $z = 2.187$ absorber towards HE 0001–2340 currently undergoes a merger event that leads to the formation of massive stellar clusters, these clusters should locally enrich their interstellar environment with heavy elements by supernova explosions. Such circum-cluster environments, when they are young, should not have had enough time to mix with the more extended interstellar environment of the host galaxy. This possibly creates distinct regions with enhanced heavy-element abundances similar to what is observed in components O and P. The sub-DLA towards HE 0001–2340 thus may represent a young galaxy at $z \approx 2$ that is forming due to merging.

6. Summary

We have performed a detailed analysis of the sub-DLA at $z = 2.187$ towards HE 0001–2340 and have derived the following results:

- (1) We identify 16 absorption subcomponents in neutral and weakly ionized species (H I, D I, C II, N I, N II, O I, Mg II, Al II, Al III, Si II, P II, and Fe II), and 25 subcomponents in C IV and Si IV. These components span a velocity range of ~ 400 km s⁻¹ in the $z = 2.187$ restframe. The

system has a total neutral hydrogen column density of $\log N(\text{H I}) \approx 19.7$.

- (2) The overall abundance of the absorber is $[\text{M}/\text{H}] = -1.81 \pm 0.07$ dex (1/65 solar), as derived from unsaturated O I absorption in the strongest neutral gas component A at $v_{\text{rel}} = +13 \text{ km s}^{-1}$ (relative to $z = 2.187$). The lack of depletion of Si II and the absence of molecular hydrogen imply that the absorber is devoid of dust.
- (3) The gas in component A shows a classic massive star abundance pattern with little sign of primary nitrogen. Taking possible ionization effects into account, we estimate $[\text{N}/\text{H}] \lesssim -3.3$ and $[\text{N}/\text{O}] \lesssim -1.5$. These values place the $z = 2.187$ absorber among systems with the lowest measured $[\text{N}/\alpha]$ ratios in astrophysical sites so far. This result is in line with the idea that the first stars in the Universe have enriched the intergalactic medium to a level of $[\text{N}/\alpha] \approx -1.5$.
- (4) Components O and P near -350 km s^{-1} exhibit significant overabundances of phosphorus, silicon, and aluminum ($[\text{P}/\text{C}] \approx +1.5$, $[\text{Si}/\text{C}] \approx +0.6$ and $[\text{Al}/\text{C}] \approx +0.5$) after applying an ionization correction. Possibly, the gas belonging to these components is locally enriched by the supernova ejecta from one or more massive stellar clusters. Absorption by DI is possibly detected in components O and P in the blue wings of the H I Ly α , Ly β and Ly γ lines. However, our analysis of these lines leads to an extraordinarily high D/H ratio of $\geq 1.22 \times 10^{-4}$, implying that the DI absorption is blended with an H I interloper.
- (5) We suggest that the large number of absorption components spread over several hundred km s^{-1} indicates the merging of two galaxies or protogalactic structures. This merging eventually triggers the formation of star clusters that are responsible for the abundance anomalies observed in components O and P. If so, the sub-DLA towards HE 0001–2340 may represent a young galaxy at $z \approx 2$ that is forming out of a merger event.

Acknowledgements. This work is based on observations collected during program 166.A-0106 (PI: Jacqueline Bergeron) of the European Southern Observatory with the Ultraviolet and Visible Echelle Spectrograph mounted on the 8.2 m KUEYEN telescope operated at the Paranal Observatory, Chile. We are grateful to the astronomers that have performed the observations in service mode. P.R. is supported by the German *Deutsche Forschungsgemeinschaft*, DFG, through Emmy-Noether grant Ri 1124/3-1.

Appendix A: Comments on deuterium

The H I profile fit described in Sect. 3.3 (Fig. 5) suggests the presence of additional absorption in the blue wing of the Ly α , Ly β and Ly γ profiles – exactly at the position where DI absorption from the two bluer-most components O and P is expected. A Voigt-profile fit to the possible DI Ly β and Ly γ absorption (shown in Fig. A.1) provides $\log N(\text{D I})_{\text{O}} = 13.94 \pm 0.04$ and $\log N(\text{D I})_{\text{P}} = 13.54 \pm 0.05$ together with $b(\text{D I})_{\text{O}} = 10.8 \pm 1.7$ and $b(\text{D I})_{\text{P}} = 11.6 \pm 1.9$. The values for $\log N(\text{D I})$ do not change significantly if one assumes lower b values. With $N(\text{H I})_{\text{OP}} \leq 18$ (see Sect. 3.3), we derive a limit for the deuterium-to-hydrogen ratio of $(\text{D}/\text{H})_{\text{OP}} \geq 1.22 \times 10^{-4}$.

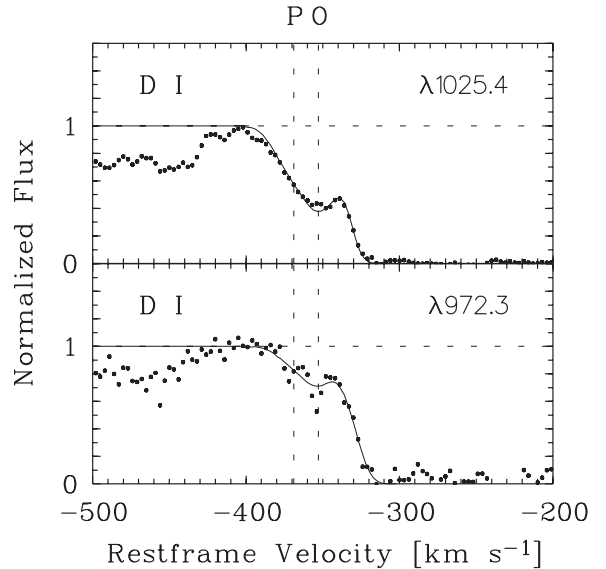


Fig. A.1. DI Ly β , and Ly γ absorption in the $z = 2.187$ absorber. The solid line represents the best fit to the data with $\log N(\text{D I}) = 13.94 \pm 0.04$ for component O and 13.54 ± 0.05 for component P assuming $b = 10.8 \pm 1.7 \text{ km s}^{-1}$ and $11.6 \pm 1.9 \text{ km s}^{-1}$, respectively.

This is ~ 4 times higher than the canonical value for chemically young gas (3.0×10^{-5} ; e.g., Burles et al. 2001). The simplest and most likely explanation for this unusually high (D/H) ratio is to assume that the deuterium lines in components O and P are blended with an “hydrogen interloper”, a weak H I absorber that would be located near -440 km s^{-1} (in the $z = 2.187$ rest-frame) and that coincidentally falls together with the DI absorption in components O and P. However, as recently reviewed by Jedamzik (2002), there are a number of possible production mechanisms at high z that may *locally* enhance the (D/H) ratio in certain environments, e.g., in regions predominantly enriched by supermassive stars. It is an intriguing coincidence that the apparently enhanced (D/H) ratio in the $z = 2.187$ absorber toward HE 0001–2340 is observed in gas that exhibits abundance anomalies also in other elements (P, Si, and Al; see Sect. 4.2). We therefore have to acknowledge that the existence of an intrinsically enhanced (D/H) ratio in components O and P cannot be entirely excluded, although the presence of an hydrogen interloper certainly remains the most likely explanation for the apparent (D/H) anomaly.

References

- Allende Prieto, C., Lambert, D. L., & Asplund, M. 2001, *ApJ*, 556, L63
 Burles, S., Nollet, K. M., & Turner, M. S. 2001, *ApJ*, 552, L1
 Centurión, M., Molaro, P., Vladilo, G., et al. 2003, *A&A*, 403, 55
 Dessauges-Zavadsky, M., Péroux, C., Kim, T.-S., D’Odorico, S., & McMahon, R. G. 2003, *MNRAS*, 345, 447
 D’Odorico, V., & Petitjean, P. 2001, *A&A*, 370, 729
 Ferland, G. 1996, Hazy, a Brief Introduction to CLOUDY 90, Univ. Kentucky Phys. Dept. Int. Rep.
 Fontana, A., & Ballester, P. 1995, *ESO Messenger*, 80, 37
 Israelian, G., Ecuivillon, A., Rebolo, R., et al. 2004, *A&A*, 421, 649
 Izotov, Y. I., & Thuan, T. X. 1999, *ApJ*, 511, 639
 Jedamizik, K. 2002, *Ap&SS*, 50, 1239

- José, J., Coc, A., & Hernanz, M. 2003, *ApJ*, 560, 897
- Knierman, K. A., Gallagher, S. C., Charlton, J. C., et al. 2003, *AJ*, 126, 1227
- Lanzetta, K. M., Wolfe, A. M., & Turnshek, D. A. 1995, *ApJ*, 440, 435
- Ledoux, C., Petitjean, P., & Srianand, R. 2003, *MNRAS*, 346, 209
- Lu, L., Sargent, W. L. W., Barlow, T. A., Churchill, C. W., & Vogt, S. S. 1996, *ApJS*, 107, 475
- Madau, P., Haardt, F., & Rees, M. J. 1999, *ApJ*, 514, 648
- Morton, D. C. 2003, *ApJS*, 149, 205
- Nakamura, T., Umeda, H., Iwamoto, K., et al. 2001, *ApJ*, 555, 880
- Nussbaumer, H., & Storey, P. J. 1986, *A&AS*, 64, 545
- Péroux, C., Dessauges-Zavadsky, M., D’Odorico, S., Kim, T.-S., & McMahon, R. G. 2003, *MNRAS*, 345, 480
- Petitjean, P., Rauch, M., & Carswell, R. F. 1994, *A&A*, 291, 29
- Petitjean, P., Srianand, R., & Ledoux, C. 2002, *MNRAS*, 332, 383
- Pettini, M., Ellison, S., Bergeron, J., & Petitjean, P. 2002, *A&A*, 391, 21
- Prochaska, J. X., Henry, R. B. C., O’Meara, J. M., et al. 2002, *PASP*, 114, 933
- Prochaska, J. X., Howk, J. C., & Wolfe, A. M. 2003, *Nature*, 423, 57
- Prochaska, J. X., & Wolfe, A. M. 1999, *ApJS*, 121, 369
- Richter, P., Sembach, K. R., Wakker, B. P., et al. 2001, *ApJ*, 559, 318
- Schweizer, F., & Seitzer, P. 1998, *AJ*, 116, 2206
- Shields, G. A. 1996, *ApJ*, 461, L9
- Smith, G. H., & Kraft, R. P. 1996, *PASP*, 108, 344
- Sofia, U. J., & Jenkins, E. B. 1998, *ApJ*, 499, 951
- Umeda, H., & Nomoto, K. 2004, *Nature*, 422, 871
- Vladilo, G., Centurión, M., Bonifacio, P., & Howk, J. C. 2001, *ApJ*, 543, 24
- Wolfe, A. M., Lanzetta, K. M., Foltz, C. B., & Chaffee, F. H. 1995, *ApJ*, 454, 698